OFFICE OF NAVAL RESEARCH

Contract: N00014-85-K-0222

Work Unit: 4327-555

Scientific Officer: Dr. Richard S. Miller

Technical Report No. 24

STRENGTH UNDER VARIOUS MODES OF DEFORMATION

by

C. W. Extrand and A. N. Gent

Institute of Polymer Engineering
The University of Akron
Akron, Ohio 44325

May, 1990

SECURITY CLASSIFICATION OF THIS PAGE (When Data Entered)

REPORT DOCUMENTATION PAGE		READ INSTRUCTIONS BEFORE COMPLETING FORM
1. REPORT NUMBER Technical Report No. 24	2. GOVT ACCESSION NO.	3. RECIPIENT'S CATALOG NUMBER
4. TITLE (and Subtitle) Strength Under Various Modes of Deformation		5. TYPE OF REPORT & PERIOD COVERED Technical Report 6. PERFORMING ORG. REPORT NUMBER
7. AUTHOR(s) C. W. Extrand and A. N. Gent		8. CONTRACT OR GRANT NUMBER(s) N00014-85-K-0222
9. PERFORMING ORGANIZATION NAME AND ADDRESS Institute of Polymer Engineering The University of Akron Akron, OH 44325-0301		10. PROGRAM ELEMENT, PROJECT, TASK AREA & WORK UNIT NUMBERS 4327-555
11. CONTROLLING OFFICE NAME AND ADDRESS Office of Naval Research Power Program Arlington, VA 22217-5000		12. REPORT DATE May 1990 13. NUMBER OF PAGES 48
14. MONITORING AGENCY NAME & ADDRESS(if different from Controlling Office)		15. SECURITY CLASS. (of this report) 15a. DECLASSIFICATION/DOWNGRADING SCHEDULE

16. DISTRIBUTION STATEMENT (of this Report)

According to attached distribution list.
Approved for public release; distribution unrestricted.

17. DISTRIBUTION STATEMENT (of the abstract entered in Block 20, if different from Report)

18. SUPPLEMENTARY NOTES

Submitted to: International Journal of Fracture

19. KEY WORDS (Continue on reverse side if necessary and identify by block number)

Crack Growth, Elastomers, Equi-Biaxial, Fracture Energy, Rubber, Tear Strength, Tensile Strength, Surface Tension, Hot Strength, Mechanics, → Mat... (—JG)

20. ABSTRACT (Continue on reverse side if necessary and identify by block number)

Breaking stresses and strains have been measured for sheets of a brittle elastic material, a highly crosslinked polyisoprene rubber, under three different modes of deformation: simple tension, pure shear, and equi-biaxial extension. Sharp cracks, about 2 mm long, were made in the center of each specimen before testing. The breaking stress for equi-biaxial straining was found to be significantly higher than

(over)

DD FORM 1 JAN 73 1473 EDITION OF 1 NOV 65 IS OBSOLETE
S/N 0102-LF-014-6601

SECURITY CLASSIFICATION OF THIS PAGE (When Data Entered)

NEXT Page →

for uniaxial straining while the breaking strain was about one-half as large. All of the results are in accord with a single value of the fracture energy, about 150 J/m^2

Strength Under Various Modes of Deformation

C.W. Extrand and A.N. Gent

Polymer Engineering Center

The University of Akron

Akron, Ohio, 44325-4001

Abstract

Breaking stresses and strains have been measured for sheets of a brittle elastic material, a highly crosslinked polyisoprene rubber, under three different modes of deformation: simple tension, pure shear, and equi-biaxial extension. Sharp cracks, about 2 mm long, were made in the center of each specimen before testing. The breaking stress for equi-biaxial straining was found to be significantly higher than for uniaxial straining while the breaking strain was about one-half as large. All of the results are in accord with a single value of the fracture energy, about 150 J/m^2.

1. Introduction

Although the relative strength of materials under different deformations is an important practical issue, there is little agreement on the answer, even in the simplest cases. Shortly after Griffith's classic paper on fracture (1), Wolf deduced that the distribution of applied stress will affect the breaking stress (2). Since then, various theoretical studies have suggested that the breaking stress in biaxial extension will be: no different from (3-5), less than (6), or greater than(7,8), that in simple tension. Other analyses suggest the

biaxial breaking stress may be greater or less than that in simple tension, depending on the value of Poisson's ratio for the material (2,9,10). Experimental studies are equally confusing, as discussed later.

In the following section, some important theoretical and experimental studies of the strength of solids under multi-axial loading are summarized. Some new measurements are then presented for sheets of a brittle elastic material, a highly-crosslinked cis-polyisoprene elastomer, containing a small through-crack in the center of the sheets, and stressed to break in uniaxial tension, constrained tension (pure shear) and equi-biaxial tension. Measurements were attempted both for sheets that were much thinner than the length of the crack and for sheets that were somewhat thicker, corresponding to conditions approaching plane stress and plane strain, respectively.

2. Previous Work

(a) Theoretical studies

When discussing biaxial stressing of a sheet containing a center crack, a biaxiality ratio $\underline{k}$ is often employed to relate the applied far-field stress parallel to the crack (x-axis) to the far-field stress perpendicular to the crack (y-axis)

$$k = \sigma_x/\sigma_y. \qquad (1)$$

When $\underline{k} = 1$, the deformation is equi-biaxial tension and when $\underline{k} = 0$, the

deformation is a simple tension with the stress applied along the y-axis.

Griffith originally derived the breaking stress of a sheet containing a center crack under equi-biaxial tension (1)

$$\sigma_b^2 = 4EG/\pi a(1 + \nu)(3 - \kappa) \qquad (2)$$

where E is the tensile (Young) modulus of the material, G is the critical strain-energy-release rate or fracture energy, 2a is the crack length, and ν is Poisson's ratio. For plane stress, $\kappa = (3 - \nu)/(1 + \nu)$, and for plane strain, $\kappa = 3 - 4\nu$. Griffith later corrected this result (11), giving the now widely-accepted relation for the breaking stress in simple tension,

$$\sigma_b^2 = 4EG/\pi a(1 + \nu)(1 + \kappa). \qquad (3)$$

Thus, under plane stress conditions,

$$\sigma_b^2 = EG/\pi a \qquad (4)$$

and in plane strain,

$$\sigma_b^2 = EG/\pi a(1 - \nu^2). \qquad (5)$$

No distinction was made between equi-biaxial and uniaxial loading; the breaking stresses were apparently assumed to be equal.

Swedlow derived a general expression for the breaking stress under multi-axial loading (9). For biaxial loading it reduces to a form first derived by Wolf (2):

$$\sigma_b^2 = (8EG/3\pi a)(1 + \nu)/[(3\nu - 1)k + (1 + \nu)] \qquad (6)$$

for plane stress, and

$$\sigma_b^2 = (8EG/3\pi a)/[(4\nu - 1)k + 1] \qquad (7)$$

for plane strain.

For an incompressible material such as rubber ($\underline{\nu} = 1/2$) in simple tension ($\underline{k} = 0$), these expressions both reduce to

$$\sigma_b^2 = 8EG/3\pi a. \qquad (8)$$

This differs from the Griffith forms for simple tension, Equations 4 and 5, by factors of 8/3 and 2. The cause of these discrepancies is not known to the present authors.

Figure 1 shows the relationship derived by Swedlow between breaking stress ratio $\underline{R}$ (= $\underline{\sigma_b}$ in biaxial tension / $\underline{\sigma_b}$ in uniaxial tension) and biaxiality ratio $\underline{k}$, in plane stress. When Poisson's ratio $\underline{\nu}$ is less than 1/3, the breaking stress in biaxial tension is predicted to be greater than in uniaxial tension, and when $\underline{\nu}$ is greater than 1/3 the situation is reversed. Similar conclusions are reached in plane strain. For most engineering materials, therefore, the

breaking stress in biaxial extension would be expected to be about the same as, or less than, that in simple tension. For example, aluminum with Poisson's ratio of about 0.3 would have a breaking stress in simple tension slightly greater in plane stress and slightly less in plane strain than under equi-biaxial loading. For plane stress and strain, both polymethyl methacrylate (PMMA), with $\nu \approx 0.4$, and rubber, with $\nu \approx 0.5$, would be expected to show a lower breaking stress in biaxial extension than in simple tension.

Eftis and Jones (10) derived expressions for the breaking stress of biaxially-loaded sheets containing a center crack, similar to those of Wolf (2) and Swedlow (9). The breaking stress σ_b also depended upon the value of Poisson's ratio of the material and the biaxiality ratio. When $\nu = 1/2$, the theoretical predictions of Swedlow (9) and Eftis and Jones are identical. For other values of Poisson's ratio, the two differ only slightly.

However, other studies have yielded quite different conclusions. For example, Sih and Liebowitz (5) derived the strain energy of a stressed sheet containing an elliptical crack and found that for both equi-biaxial and constrained tension (pure shear) loading, the breaking stress was less than that in uniaxial tension. But, as the shape of the elliptical hole approached that of a linear crack, both the biaxial and pure shear breaking stresses approached the value for uniaxial loading, given by Griffith. Thus, Sih and Liebowitz concluded that there is no difference in the breaking stresses for uniaxial, pure shear, or equi-biaxial loading of a material with a linear center crack. Kassir and Sih (4) considered a solid block containing a

central flat "penny-shaped" crack, loaded multi-axially, and also found that the breaking stress was unaffected by stresses applied parallel to the crack.

Thus, apparently similar theoretical studies have arrived at divergent conclusions.

Other studies have dealt with special cases and suggest that breaking stresses under various loading conditions will differ. For example, Adams (7) employed a hypothesis that fracture occurs at a critical crack opening displacement. Loading parallel to the crack introduces an additional constraint on crack opening, which increases with the value of Poisson's ratio. Adams argued that, in consequence, additional stresses are required to open the crack sufficiently to cause failure, so that the breaking stress σ_b will increase linearly with the biaxiality ratio k, and the larger the value of Poisson's ratio, the greater will be the effect.

For a material undergoing plastic deformation before fracture, Hilton (8) predicted the breaking stress to increase under biaxial loading, even when the yield zone was comparatively small, while compressive loading parallel to the crack was predicted to have the opposite effect. Thus, these two treatments of non-linear materials both suggest that the biaxial breaking stress will be higher.

The various theoretical conclusions about the breaking stress ratio are summarized in Table 1. Kassir and Sih (4) and Sih and Liebowitz (5) concluded that there would be no difference between the breaking stresses in biaxial and uniaxial loading. Wolf (2), Swedlow (9) and Eftis and Jones (10) predicted that the breaking stress in most

materials would be less in equi-biaxial loading than in simple tension. Adams (7) and Hilton (8) predicted that it would be greater.

(b) Experimental studies of biaxial strength

Only a few experimental measurements are known to the authors of breaking stress in deformations other than simple tension. They are listed here.

(i) Biaxial strength of aluminum

Kibler and Roberts (12) measured the strength of biaxially-loaded sheets of 6061-T4 and 6061-T6 aluminum alloys. Both materials showed an increase in fracture toughness K with increasing load biaxiality k (σ_b is proportional to K). Eftis and Jones (10) carried out similar measurements on specimens of 7075-T6 aluminum alloy having center cracks both parallel and perpendicular to the rolling direction of the sheet. In both cases the breaking stress increased slightly with increasing load parallel to the crack. Thus, the breaking stress of aluminum appears to be somewhat greater in biaxial loading than in uniaxial loading.

(ii) Biaxial strength of PMMA

Kibler and Roberts (12) measured the strength of biaxially-loaded sheets of PMMA (polymethyl methacrylate) using square-sided and cruciform specimens. A load parallel to the crack caused the breaking stress of the material to rise. On the other hand, Leevers, Culver, and Radon (13) found in a preliminary study that the fracture toughness

K of PMMA sheets with a center crack decreased slightly with increasing load parallel to the crack direction. In a later study, however, Radon, Leevers, and Culver (14) concluded that stress parallel to the crack direction had no appreciable effect on the breaking stress. In contrast, Eftis and Jones (10) concluded that the fracture toughness K decreased with increasing biaxiality k. But their data had a great deal of scatter. It is therefore difficult to decide from these conflicting studies whether the effect of biaxial loading on the strength of PMMA is significant or not, and if it is, whether the breaking stress is larger or smaller under equi-biaxial loads than under simple tension.

Although aluminum and PMMA are technically important materials, they are rather poor choices for experiments designed to test the predictions of linear-elastic fracture mechanics. Aluminum has a low yield stress and PMMA is prone to stress crazing, a form of plastic deformation, before fracture.

(iii) Biaxial strength of rubber

Smith and Rinde (15) measured the breaking stresses for rubber tubes under combined extension and inflation, and concluded that the breaking stress in constrained biaxial extension was somewhat higher than in simple tension. Dickie and Smith (16) studied the fracture of inflated circular membranes and concluded that the breaking stress in equi-biaxial tension was considerably higher than in simple tension.

One should note, however, that failure of tubes and membranes generally starts from the surface, where flaws are less damaging,

whereas failure of strips in tension generally starts from an edge, where flaws are both more common and more serious. Thus, it is not known at present whether simple sheets of simple elastic solids are really stronger in equi-biaxial extension than in uni-axial tension when the flaw from which failure initiates is the same in both cases.

We have therefore measured the breaking stress and breaking strain for sheets of a brittle elastic material, a highly-crosslinked polyisoprene rubber, with a small cut made in the center of the sheets, under three different modes of deformation: uniaxial extension, constrained extension (pure shear), and equi-biaxial extension. Measurements were attempted both for sheets that were much thinner than the cut length and for sheets that were somewhat thicker, corresponding to conditions approaching plane stress and plane strain, respectively. The results are reported here.

Because the highly-crosslinked rubber used was quite brittle, samples with a center cut failed at unusually small strains for rubber — less than 20%. As a result, the stress - strain relations were approximately linear up to the breaking point. The elastic behavior in simple tension is shown in Figure 2 for a parallel-sided strip with no crack. In this case the breaking elongation was appreciably higher, about 25%, and the stress - strain relation was slightly non-linear. From the linear relation obtained at small strains, the value of the tensile (Young) modulus E of this material was found to be 2.3 MPa.

2. Experimental Details

(a) Material and test apparatus

The material used in this study was Goodyear Natsyn 2200 polyisoprene. It was molded and crosslinked in the form of thin sheets, about 1 and 2.6 mm thick, by adding 5 per cent by weight of dicumyl peroxide (Dicup-R, Hercules Chemical Company) and heating the mixture for 50 minutes at 150°C in a sheet mold in an electrically-heated press.

Stress-strain relations in uni-axial tension and constrained tension (pure shear) were measured using an Instron tensile test machine. For equi-biaxial deformations, a thin-film biaxial stretcher, Model BIX-702, manufactured by Iwamoto Seisakusho Co., Ltd. of Kyoto, Japan, was used. This apparatus can apply loads of up to 100 kg in each direction, with a maximum displacement of 500 mm. The arrangement employed to hold the sample is shown schematically in Figure 3. It consisted of forty pneumatically-controlled clamps, each of 1 cm width: nine on each side and four at the corners. The apparatus is designed so that the clamps separate at a constant rate to produce a uniform strain field.

Stretching forces were measured by two load cells, one for each direction, attached to the center clamps on two adjacent sides, Figure 3. They were calibrated using an arrangement of pulleys and weights, both with the clamps moving as well as stationary.

All experiments were carried out at room temperature, about 23°C.

(b) Test specimens and procedures

(i) Tearing

Tear experiments were carried out using rectangular strips, 150 mm long and 30 mm wide, cut from the molded sheets. The strips were cut along the centerline for a distance of about 50 mm and the two legs created in this way were then pulled apart in opposite directions at various rates, causing a tear to propagate along the centerline, Figure 4. The fracture energy G was calculated from the average force F required to propagate a tear and the width of the tear w, $G = 2F/w$ (17). It should be noted that the width w was about 40% greater than the thickness of the rubber sheet because the tear tended to run at an angle of about 45° to the plane of the sheet (18,19).

Fracture energies were determined for rates of tearing ranging from 8 μm/s to 8 mm/s.

(ii) Uniaxial tension

Testpieces for uniaxial tension experiments were cut with a dumbell-shaped die to have a central parallel-sided length of 40 mm and a width of 13 mm. A through-crack was made in the center of the specimen, at right angles to the stretching direction, using a small sharp metal spear, lubricated with soapy water. By pushing the widest part of the spear head all the way though the rubber sheet, a cut of uniform length was obtained. The cut length $2a$ for six sheets was measured using a travelling microscope to be 1.906 ± 0.005 mm.

The effect of crack size was examined using tensile samples with center cuts of different length, made using spears of different widths. Samples were suspended from the top clamp of the tensile test machine and the bottom clamp was then tightened. As it was tightened, it compressed the material within it and caused some to extrude,

lengthening the portion between the clamps. As a result, the initial tensile force $\underline{F}$ on the sample changed from zero to a small negative, i.e., compressive value. To correct for this, the sample was extended slightly to bring the initial force reading back to zero. The separation of the clamps was measured at this point and taken as the initial length of the sample. The change in length was relatively small, about 2 percent of the breaking elongation for thin sheets and about 5 percent for thick sheets.

After failure, the width of the sample was measured with a microscope and the thickness with a dial gauge. The stress was computed from the measured force and the unstrained sample dimensions, and the strain from the crosshead displacement, relative to the initial length of the sample.

Specimens were stretched to break at a cross-head speed of 20 mm/min, corresponding to a strain rate $\dot{\underline{e}}$ of approximately 8×10^{-3} s^{-1}.

(iii) Pure shear (constrained tension)

Pure shear or constrained tension samples were molded so that both clamped edges had a thick ridge along their widths to prevent them from slipping. They had an initial length between the clamps of about 15 mm and a width of about 150 mm. A through-crack was made in the center of each sample, parallel to the width direction, as for the simple extension samples.

A sample was fastened into the upper clamp and the crosshead was adjusted to give an initial clamp separation, and hence sample length, of 15 mm. The bottom clamp was then tightened. As with uniaxial tests, this caused the force reading to drop below zero, and the sample

was therefore extended slightly to bring the initial force back to zero, by about 1 percent of the breaking elongation. The initial length of the sample was measured at this point. After failure, the sample width was measured with a ruler and the thickness with a dial gauge. Stresses were then calculated from the measured forces and sample dimensions, and strains were calculated from the displacement of the clamps, relative to the initial length of the sample.

Samples were stretched to break at a rate of 5 mm/min, resulting in a strain rate $\dot{\underline{e}}$ of 6×10^{-3} s^{-1}.

(iv) Equi-biaxial tension

A compression-molded sheet having a thickness of 1 mm was trimmed to fit the biaxial stretcher, approximately 150 mm x 150 mm. Stress-relieving holes, 4 mm in diameter were made in the rubber sheet at points lying between each clamp. Cuts were then made connecting the holes to the side of the sheet as shown in Figure 5. Each tab made in this way was reinforced before clamping it with a piece of vinyl tape. The area within the holes and tape reinforcement was about 120 mm x 120 mm. Finally, a crack was made in the center of the sheet, as described previously.

Thick biaxial samples tended to fail at the clamps rather than at the center crack. A mold was therefore made to produce sheets with smooth molded-in stress-relieving holes, about 3 mm in diameter, arranged to lie between each clamp, and with a cloth-reinforced edge for clamping. The area inside the holes was about 120 mm by 120 mm and the central square, about 100 mm by 100 mm, was made of smaller thickness to raise the stress in this region. Figure 6 shows a

cross-section of a thick biaxial sample. The central region, where the cut was placed, was approximately 2.6 mm thick.

Biaxial samples were placed in the clamp assembly and stretched at a rate of 60 mm/min to give a strain rate of 8×10^{-3} s^{-1}. After failure, the thickness was measured with a dial gauge. Stresses were computed from the measured forces and sample dimensions, and strains from the clamp displacements relative to the initial clamp separation.

4. Results and Discussion

(a) Stress-strain relations

Measured stress-strain relations for all three geometries are shown in Figures 7a and 7b, for thin and thick specimens, respectively. They are seen to be almost linear, right up to break. Breaking stresses and strains are listed in Table 2. The least constrained experimental condition, uniaxial extension, gave the largest breaking strain and the most constrained, equi-biaxial extension, gave the smallest. The variation reported in the measurements is the standard deviation from a set of samples measured under nominally identical conditions. Three or more samples were used in all cases, except for the thick biaxial samples when only two experiments were successful.

In constrained tension (pure shear), the stress-strain relations had an initial slope of 3.03 MPa, i.e., $1.32\ E$, in good agreement with the theoretical value of $4E/3$ (20). For biaxially stretched samples the initial slope was $2.07E$, in good agreement with the expected value of $2E$.

(b) Fracture Energy of the Material

Measured fracture energies G are plotted against the corresponding rates of tear propagation $\dot{c}$ in Figure 8. They showed a marked dependence on tear rate, increasing by a factor of three, from 80 to 250 J/m^2, as the tear rate increased by three orders of magnitude.

(c) Dependence of Breaking Stress on Crack Length.

The tensile breaking stress σ_b was measured for thin samples having center cuts of different lengths $2a$, ranging from 1.5 to 3.8 mm. As shown in Figure 9, the results were in satisfactory agreement with a direct proportionality between σ_b and $a^{-1/2}$, in accordance with Griffith's relation, Equation 4. The slope of the linear relation shown in Figure 9 corresponds to a value for fracture energy G of 145 ± 8 J/m^2. From the results shown in Figure 8, this corresponds to a rate of crack propagation of about 1 mm/s in tensile rupture.

(d) Rate Dependence of the Breaking Stress

The tensile breaking stress σ_b was determined as a function of strain rate over three orders of magnitude from 1.67×10^{-4} to 1.67×10^{-1} m/s, using samples 0.9 mm thick with center cuts 1.9 mm long. It was found to increase somewhat with strain rate, as shown in Figure 10, from 0.29 MPa at $\dot{e} = 1.67 \times 10^{-4} s^{-1}$ to 0.40 MPa at $\dot{e} = 1.67 \times 10^{-1} s^{-1}$. The smaller dependence on strain rate than that shown by the fracture energy, Figure 8, is in accord with Equation 4, since the breaking stress is related to the fracture energy only by a half-power dependence. Small variations in the strain rates used in the breaking experiments should therefore not affect the breaking stresses strongly.

(e) Uniaxial Samples

Thin uniaxial samples with a center cut had an average thickness of $\underline{t}$ = 1.09 ± 0.135 mm, and a ratio of cut length $\underline{2a}$ to thickness of 1.75 ± 0.22, approaching plane stress conditions. The mean breaking stress was 0.325 ± 0.018 MPa and the corresponding breaking strain was 0.147 ± 0.008.

Thick uniaxial samples had an average thickness of 2.54 ± 0.05 mm, giving a ratio of cut length to sample thickness of 0.75 ± 0.02, approaching plane strain conditions. The mean breaking stress was 0.342 ± 0.009 MPa, and the corresponding breaking strain was 0.159 ± 0.006.

Both thin and thick samples followed the same, nearly linear stress-strain relation up to break, Figure 7, but the thin samples broke at slightly lower stresses and strains.

(f) Constrained tension (pure shear)

Pure shear samples had an average thickness of 0.77 ± 0.02 mm, giving a ratio of cut length to thickness of 2.48 ± 0.07. Stress-strain relations are shown in Figure 7. The mean breaking stress was 0.374 ± 0.016 MPa and the breaking strain was 0.134 ± 0.004.

Unlike uniaxial samples, failure of pure shear samples occurred over a period of several seconds. The crack grew rapidly at first, crossing most of the width of the sample and releasing about 80 % of the initial stress, but it then slowed down and crept across the remainder of the sample width. This behavior can be understood in terms of the strain energy release rate. When the length $\underline{2a}$ of the

cut is much smaller than the sample length, the strain energy release rate G depends on $\underline{a}$ (17)

$$G = CUa \qquad (9)$$

as well as upon the strain energy density $\underline{U}$. ($\underline{C}$ is a numerical constant). Thus, failure is initially autocatalytic and the crack accelerates. But when the length of the cut is greater than the sample length $\underline{L}$, the strain energy release rate becomes (17)

$$G = UL, \qquad (10)$$

and no longer depends on the length of the crack. Finally, when the crack length is comparable to the width of the specimen, the energy density $\underline{U}$ decreases towards the value for a strip in simple extension, and the strain energy release rate is correspondingly reduced.

(g) Biaxially Stretched Samples

Thin equi-biaxial samples had an average thickness of 1.20± 0.11 mm, giving a ratio of cut length to thickness of 1.59+ 0.14. The mean breaking stress was 0.451 ± 0.010 MPa and the breaking strain was 0.074 ± 0.005.

With thick equi-biaxial tension samples, only two experiments were successful. All other samples broke from an edge flaw, rather than from the initial center crack. The sheets had a thickness of 2.57 ± 0.035 mm, giving a ratio of cut length to thickness of 0.74 ± 0.01. The mean breaking stress was 0.443 ± 0.020 MPa and the breaking strain

was 0.086 ± 0.003, nearly the same as for the thin sheets.

When a biaxially-extended sample failed, the crack grew catastrophically to the sample edges, releasing all of the stress perpendicular to the crack, but a considerable amount of strain energy remained due to the clamps holding the rubber taut in the direction parallel to the crack.

(h) Contribution to biaxial breaking stress from the reinforced perimeter

The apparent stress in the reinforcement σ_r at the breaking elongation was subtracted from the apparent strength to give a corrected value of biaxial breaking strength σ_b^*. It was determined with a sample having the center cut away, leaving a square ring. A plot of stress-strain data for a thin biaxial sheet is shown in Figure 11, together with results for the reinforced perimeter ring alone. The stress in the perimeter ring at the breaking strain of the entire sheet was only 0.025 ± 0.003 MPa, about 5 % of the breaking stress for thin sheets. A correction was made by subtracting this value from the measured breaking stress. Similarly, for thick samples the mean stress in the reinforcement ring was 0.056 ± 0.008 MPa, about 12.5 % of the measured breaking stress. Again, this value was subtracted to yield a corrected breaking stress.

For both thin and thick samples, the stress in the reinforcement rings showed an initial increase up to a strain of 2-3 % and then decreased to a constant or nearly constant value.

Comparing the corrected values of breaking stress with those for

the other two loading geometries in Table 2, they are still considerably larger than for uniaxial tension or pure shear.

(i) Strain-energy-density considerations

For uniaxial tension and pure shear samples, the strain-energy density necessary to initiate fracture is given by the area under the stress-strain curve up to break. Since the material is nearly linearly elastic, this area can be approximated by:

$$U_b = (1/2)\sigma_b e_b . \qquad (11)$$

But, when a sample is stretched equi-biaxially, strain energy is put into the sample in two directions, so the strain energy is twice the area under the stress-strain curve: $\underline{\sigma}_b \underline{e}_b$. However, as the crack grows, the region around it is not rendered stress-free: it remains in a state of simple tension as a result of the stress acting parallel to the crack. Thus, biaxial strain energy is released but strain energy in uniaxial tension remains. The change in strain-energy is

$$U_b = \sigma_b e_b - \frac{1}{2}\sigma_1 e_b \qquad (12)$$

where $\underline{\sigma}_1$ is the stress in simple tension at a strain equal to the breaking strain in biaxial stretching. Strain energy densities released at failure were computed using equation (12) and are listed in Table 3, along with computed values of strain energy densities at break for uniaxial and pure shear loading.

Values of breaking energy were also calculated from the measured

stress-strain relations, without assuming that they were linear. They were fitted with quadratic functions:

$$\sigma(e) = a_1 e + a_2 e^2, \qquad (13)$$

using a least-squares analysis to determine the fitting constants, a_1, and a_2. Values of U_b were computed by integration up to the breaking strain. They are given in Table 3. The error listed for them is the standard deviation in values obtained from separate stress-strain curves.

Since the stress-strain curves were nearly linear, values of U_b computed from the quadratic functions were almost the same as those calculated assuming linear stress-strain relations, being only from 3.2 to 9.2% higher, Table 3.

(j) Fracture Energies from Breaking Stresses and Strains

From the strain energy density at failure U_b, a value of fracture energy G can be calculated using Griffith's criterion

$$G = 2\pi a U_b \qquad (14)$$

where $2a$ is the length of the center crack. Fracture energies G for the three different deformations were calculated from values of the strain energy densities released at fracture, calculated assuming linear elastic behavior, Equations (11) and (12). They are listed in Table 4.

Within experimental error, breaking stresses in simple tension, pure shear, and the corrected values for equi-biaxial tension all correspond to the same fracture energy, $G \approx 150$ J/m^2.

On the other hand, the breaking stress was significantly larger in pure shear and equi-biaxial deformation than in simple tension. (Insert page 21a) ←

5. Conclusions

The fracture behavior of sheets of a rather brittle, rubbery material with a center through-crack has been examined in three modes of deformation: simple tension, pure shear and equi-biaxial tension. The simple tension samples, which were the least constrained, showed the largest strain at break ($e_b = 0.14$) and smallest breaking stress ($\sigma_b = 0.35$ MPa), while the highly-constrained biaxial samples had the smallest breaking strain ($e_b = 0.08$) and the largest breaking stress ($\sigma_b = 0.44$ MPa).

Thick biaxial samples failed at a somewhat lower stress than thin ones, but at a stress still larger than that for simple tension samples.

Values of the strain energy released at failure for all three modes of deformation were equivalent, within experimental error, and corresponded to a fracture energy of about 150 J/m^2, in reasonable agreement with directly measured values.

Insert on page 21 at arrow.

Values of breaking stress and strain can be calculated from equations (11), (12) and (14) for plane stress conditions, assuming linear elasticity. For imcompressible materials they are:

$$\sigma_b^2 = (4/3)\cdot EG/\pi a \qquad (15)$$

for both pure shear and equi-biaxial extension,

$$e_b^2 = (3/4)\cdot G/\pi aE \qquad (16)$$

for pure shear, and,

$$e_b^2 = (1/3)\cdot G/\pi aE \qquad (17)$$

for equi-biaxial extension. Experimental results were in reasonable agreement with these relations, when scaled with respect to values measured in simple extension, Table 5.

Acknowledgements

This work forms part of a program of research supported by the Office of Naval Research (Contract N00014-85-K-0222, Project Officer Dr.R.S.Miller). Grants-in-aid from Lord Corporation and 3M are also gratefully acknowledged.

References

1. A.A. Griffith, *Phil. Trans. Roy. Soc. (London)* A221, 163 (1920).

2. K. Wolf, *Z. angew. Math. Mech.* 3, 107 (1923).

3. A.J.M. Spencer, *Int. J. Engng Sci.* 3, 441(1965).

4. M.K. Kassir and G.C. Sih, *Int. J. Engng Sci.* 5, 899 (1967).

5. G.C. Sih and H. Liebowitz, *Int. J.* Solids Struct. 3, 1 (1967)

6. G.A. Papadopoulos, *Engng Fract. Mech.* 29, No. 5, 585 (1988).

7. N.J.I. Adams, *Engng Fract. Mech.* 5, 983 (1973).

8. P.D. Hilton, *Int. J. Fract.* 9, No. 2, 149 (1973).

9. J.L. Swedlow, *Int. J. Fract. Mech.* 1, 210 (1965).

10. J. Eftis and D.L. Jones, *Int. J. Fract.* 20, 267 (1982).

11. A.A. Griffith, *Proc. 1st Int. Congr. Appl. Mech.*, Delft, 1924, pp. 55-63.

12. J.J. Kibler and R. Roberts, *J. Engng Ind.* 92, 727 (1970).

13. P.S. Leevers, J.C. Radon, and L.E. Culver, *Polymer* 17, 627 (1976).

14. J.C. Radon, P.S. Leevers and L.E. Culver, in "Fracture 1977," Vol. 3B, Internatl. Conf. Fract., Waterloo (1977) 1113.

15. T.L. Smith and J.A. Rinde, *J. Polym. Sci.* A2, 7, 675 (1969).

16. R.A. Dickie and T.L. Smith, *J. Polym. Sci.* A2, 7, 687 (1969).

17. R.S. Rivlin and A.G. Thomas, *J. Polym. Sci.* 3, No. 3, 291 (1953)

18. W.G. Knauss, *Int. J. Fract. Mech.* 6, No. 2, 183 (1970).

19. A. Ahagon, A.N. Gent, H.J. Kim, and Y. Kumagai, *Rubber Chem. Technol.* 48, 896 (1975).

20. L.G.R. Treloar, "The Physics of Rubber Elasticity," 3rd ed., Oxford University Press, New York, 1975.

Table 1. Theoretical Values of the Ratio of Equi-biaxial to Uniaxial Breaking Stress for an Incompressible Material, from Various Authors.

Author(s)	$\sigma_{b,2}/\sigma_{b,1}$	
	plane stress	plane strain
Kassir and Sih (1967)	1	1
Sih and Liebowitz (1967)	1	1
Wolf (1923)	0.866	0.707
Swedlow (1965)	0.866	0.707
Eftis and Jones (1982)	0.866	0.707
Adams (1973)	1.5	--
Hilton (1973)	Greater than 1	--

Table 2. Breaking Stresses and Strains.

Deformation	e_b	σ_b (MPa)
Uniaxial extension		
plane stress	0.147 ± 0.008	0.325 ± 0.018
plane strain	0.159 ± 0.006	0.342 ± 0.009
Pure shear		
plane stress	0.134 ± 0.004	0.374 ± 0.016
Equi-biaxial extension		
plane stress	0.074 ± 0.005	0.451 ± 0.010
plane strain	0.086 ± 0.003	0.443 ± 0.020
Corrected equi-biaxial extension		
plane stress	--	0.425 ± 0.013
plane strain	--	0.387 ± 0.028

Table 3. Strain-Energy-Densities at Failure.

Deformation	$\underline{U}_b$* (kJ/m^3)	$\underline{U}_b$** (kJ/m^3)
Uniaxial extension		
plane stress	23.9 ± 1.3	26.1 ± 2.4
plane strain	27.2 ± 0.9	28.6 ± 1.6
Pure shear		
plane stress	25.1 ± 0.9	27.4 ± 2.5
Equi-biaxial extension		
plane stress	26.5 ± 2.4	28.2 ± 2.4
plane strain	29.4 ± 2.2	30.7 ± 2.2
Corrected equi-biaxial extension		
plane stress	24.6 ± 2.7	--
plane strain	24.6 ± 3.5	--

*From equations (11),(12) and (14)

**$U_b = \int_0^{e_b} \sigma(e)\, de$

Table 4. Tear Energies Computed from Strain-Energy-Density at Failure.

Deformation	$\underline{G}$ (J/m^2)
Uniaxial extension	
plane stress	143 ± 26
plane strain	163 ± 18
Pure shear	
plane stress	150 ± 18
Equi-biaxial extension	
plane stress	159 ± 15
plane strain	176 ± 14
Corrected equi-biaxial extension	
plane stress	147 ± 17
plane strain	147 ± 21

Table 5. Breaking Stress and Strain Ratios.

Deformation	$\underline{e}_{b,i}/\underline{e}_{b,1}$	$\underline{\sigma}_{b,i}/\underline{\sigma}_{b,1}$
Uniaxial extension		
plane stress	1	1
plane strain	1.08 ± 0.10	1.05 ± 0.08
Pure shear		
plane stress	0.911 ± 0.080	1.15 ± 0.11
Equi-biaxial extension		
plane stress	0.503 ± 0.059	1.39 ± 0.11
plane strain	0.582 ± 0.051	1.36 ± 0.14
Corrected equi-biaxial extension		
plane stress	--	1.31 ± 0.11
plane strain	--	1.19 ± 0.15

Figure Legends

Figure 1. Ratio R of breaking stresses vs biaxiality ratio k of the applied stresses, from Swedlow's results for plane stress (9).

Figure 2. Relation between tensile stress σ and extension e for a parallel-sided strip of the test material. The break point is denoted by a circle.

Figure 3. Clamping arrangement for equi-biaxial extension.

Figure 4. Measurement of tear force F and tear width w.

Figure 5. Method of clamping sheets for equi-biaxial extension.

Figure 6. Cross-section of a thick molded sheet, as used for equi-biaxial extension.

Figure 7. Experimental relations between stress σ and extension e in equi-biaxial extension (E-B), pure shear (P.S.), and simple tension (S.T.). The points denote fracture.

(a) Relatively thin sheets, giving approximately plane stress conditions.

(b) Relatively thick sheets, giving approximately plane strain conditions.

Figure 8. Fracture energy $\underline{G}$ from tearing experiments as a function of rate $\dot{\underline{c}}$ of tear propagation.

Figure 9. Tensile breaking stress $\underline{\sigma}_b$ vs. crack half-length $\underline{a}$, plotted in accordance with Equation 4.

Figure 10. Tensile breaking stress $\underline{\sigma}_b$ vs. rate $\dot{\underline{e}}$ of extension.

Figure 11. Stress-strain relation for a thick sheet in equi-biaxial tension (E-B) and apparent stress for the outer ring alone.

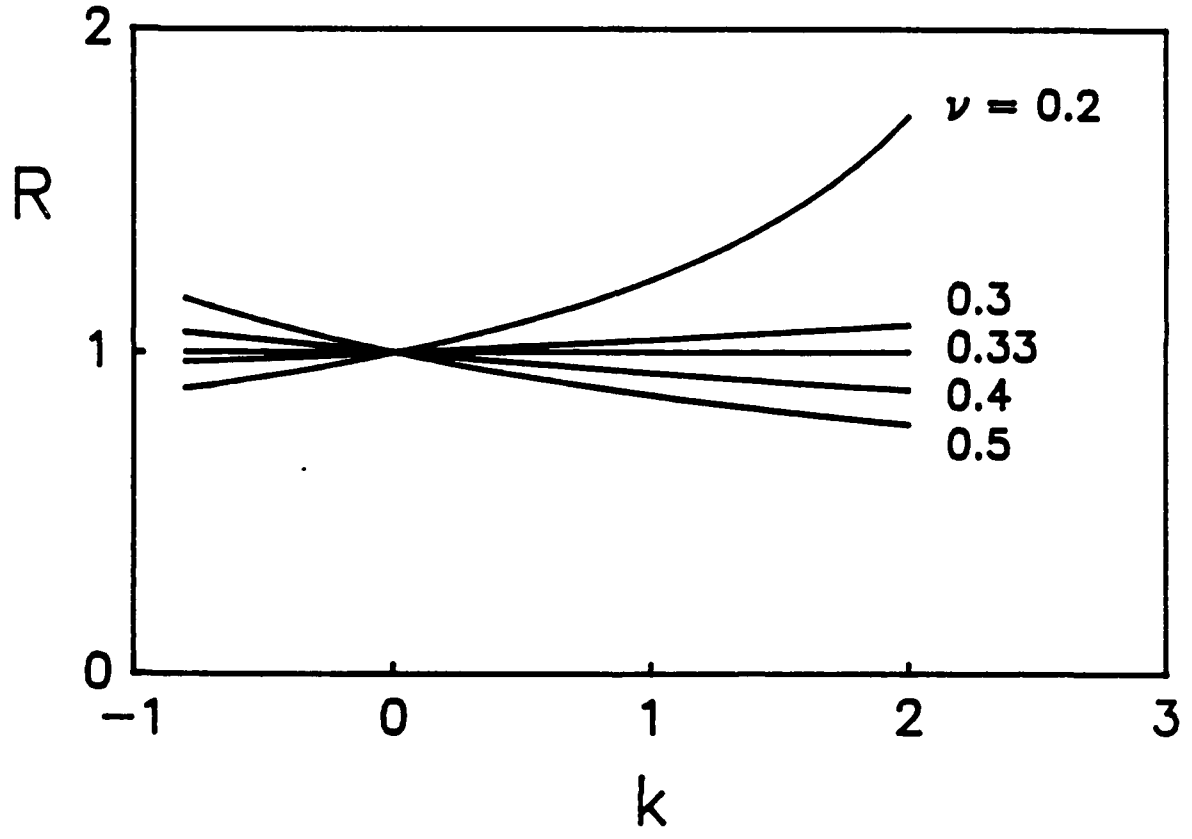

FIGURE 1

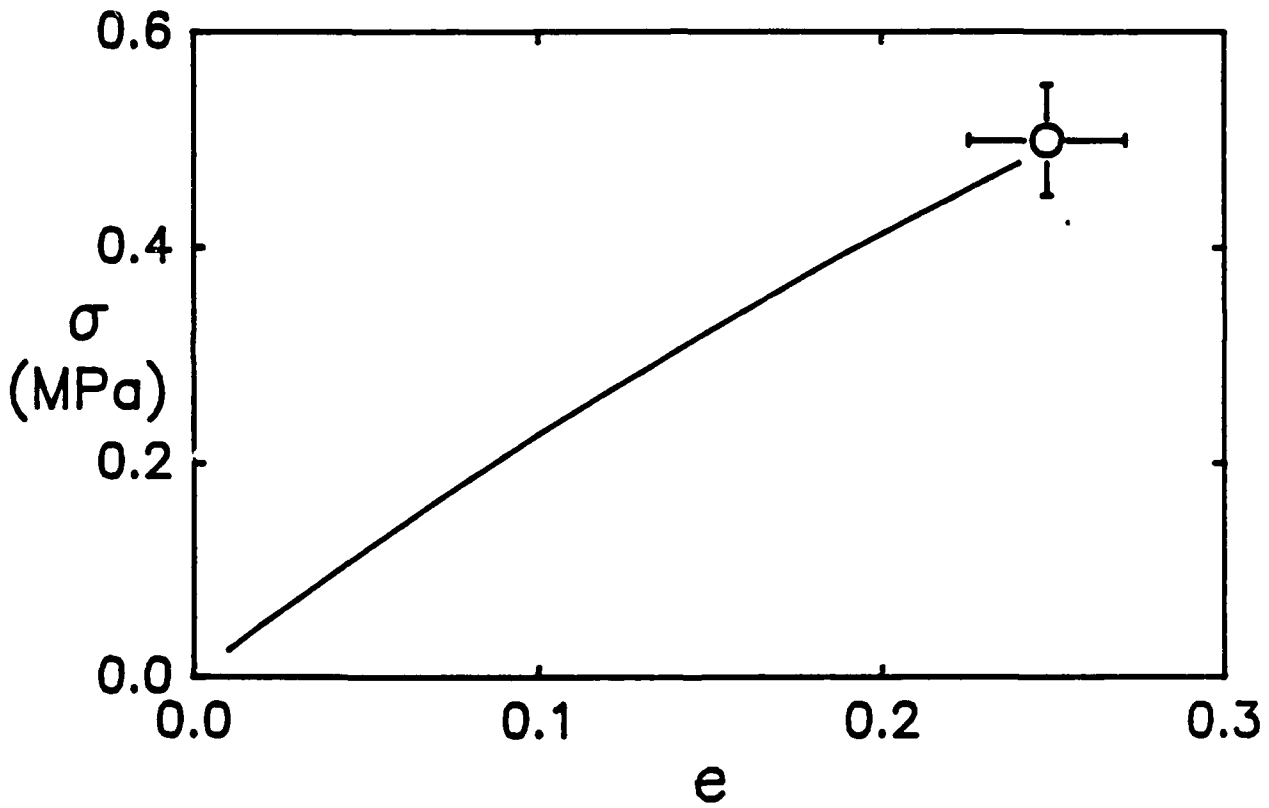

FIGURE 2

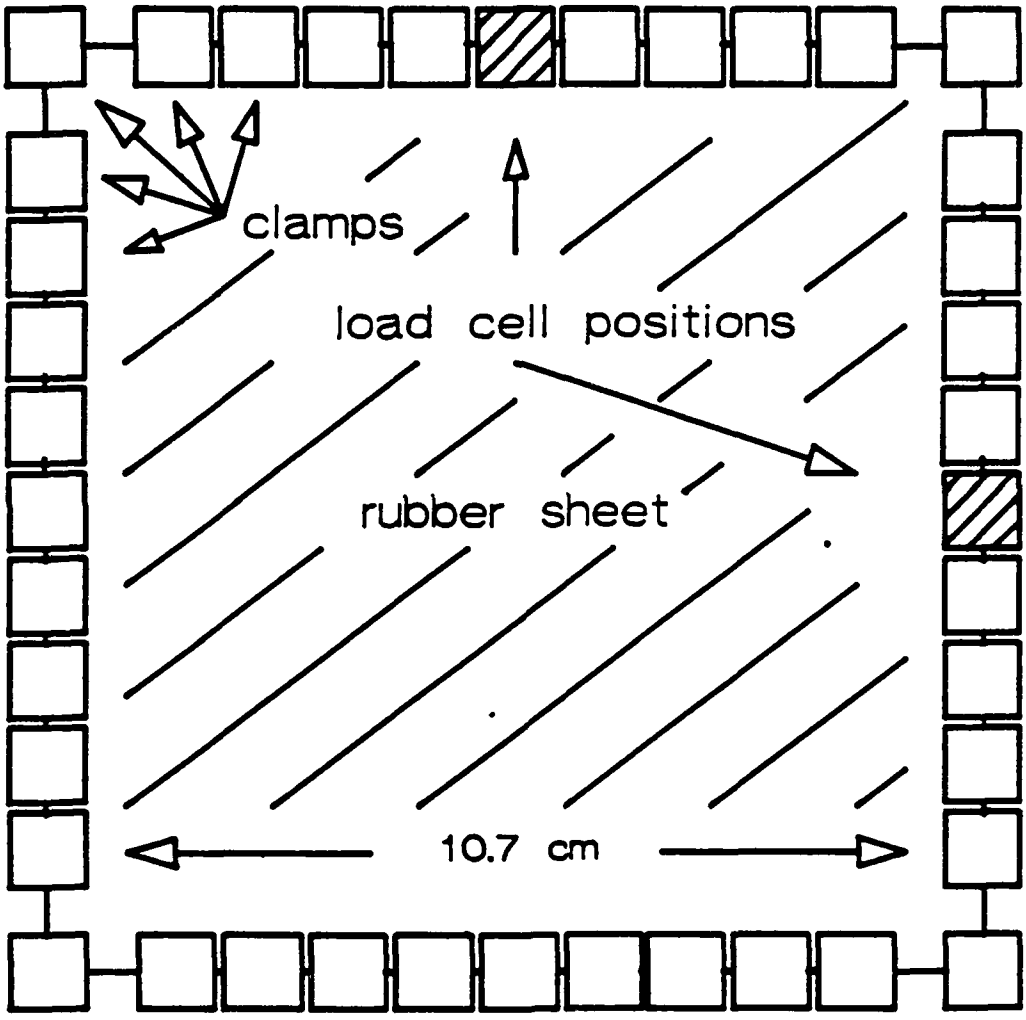

FIGURE 3

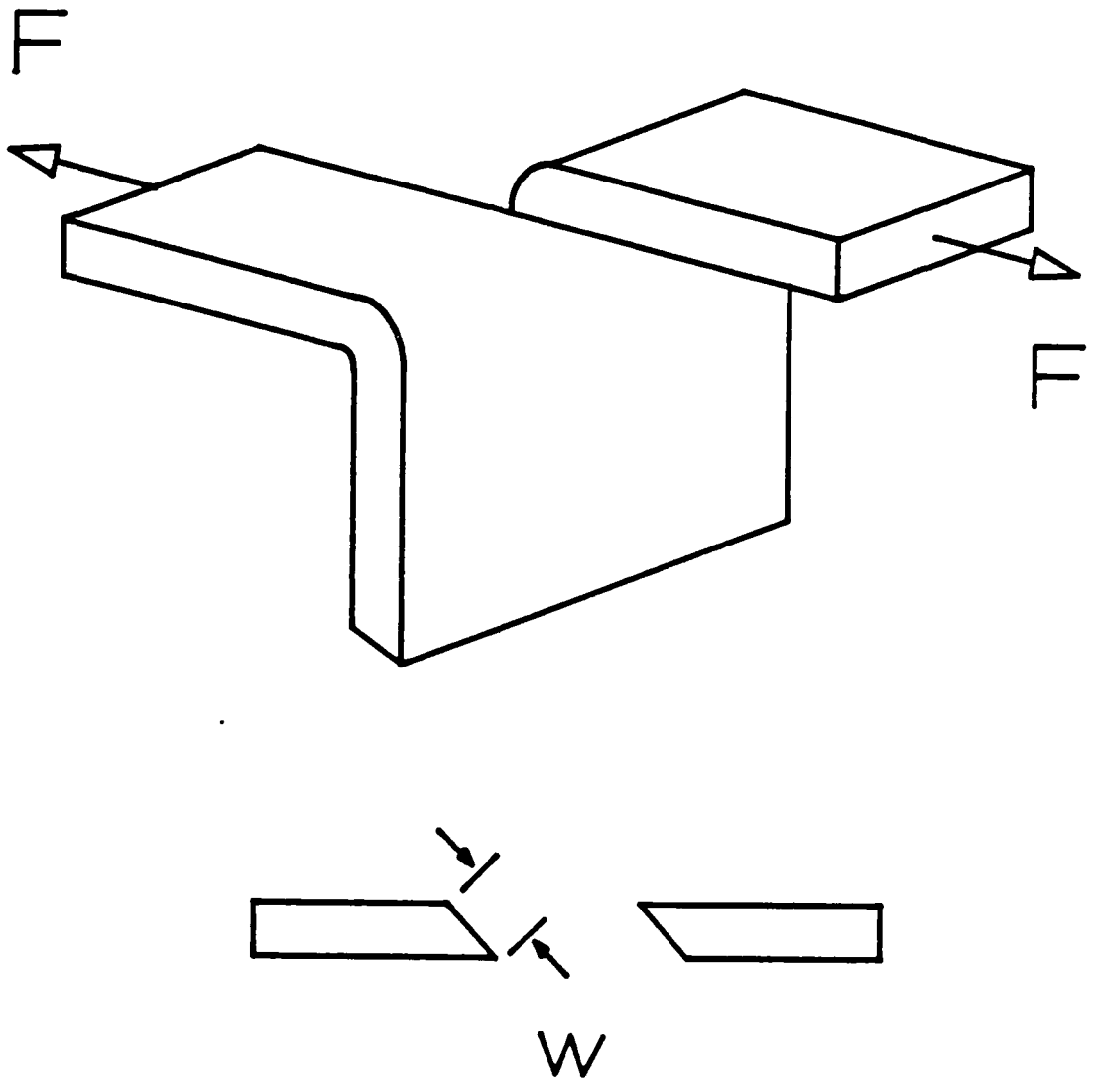

FIGURE 4

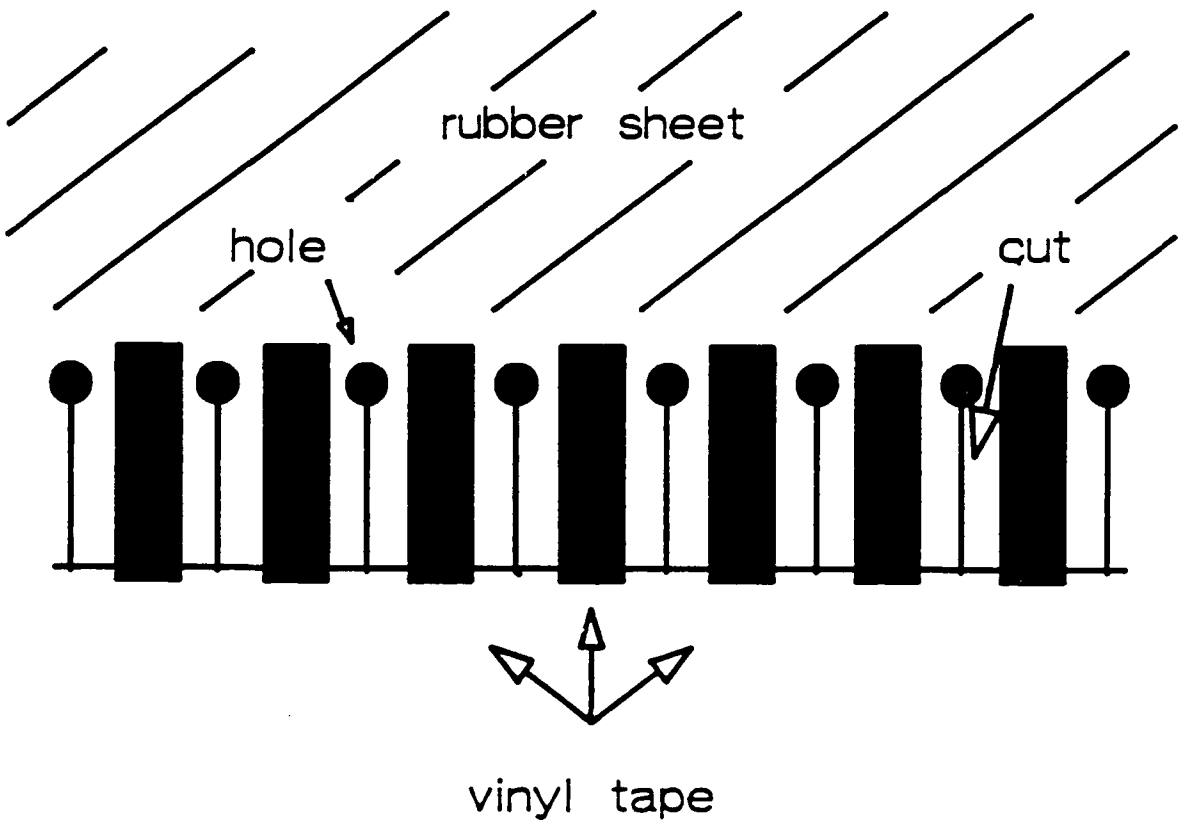

FIGURE 5

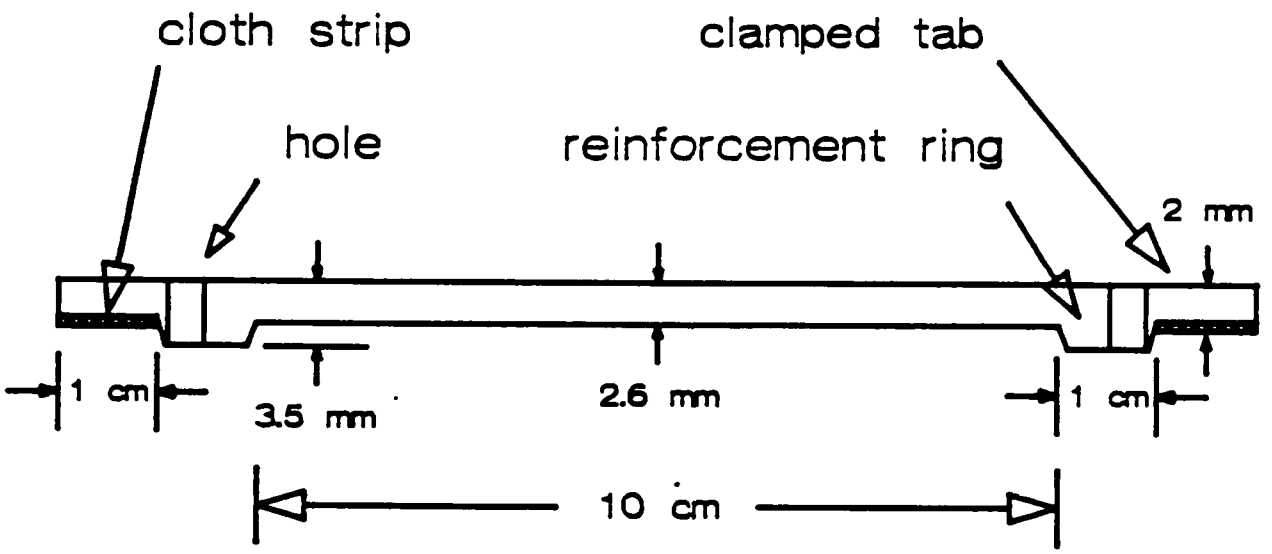
cloth strip
clamped tab
hole
reinforcement ring
2 mm
1 cm
3.5 mm
2.6 mm
1 cm
10 cm

FIGURE 6

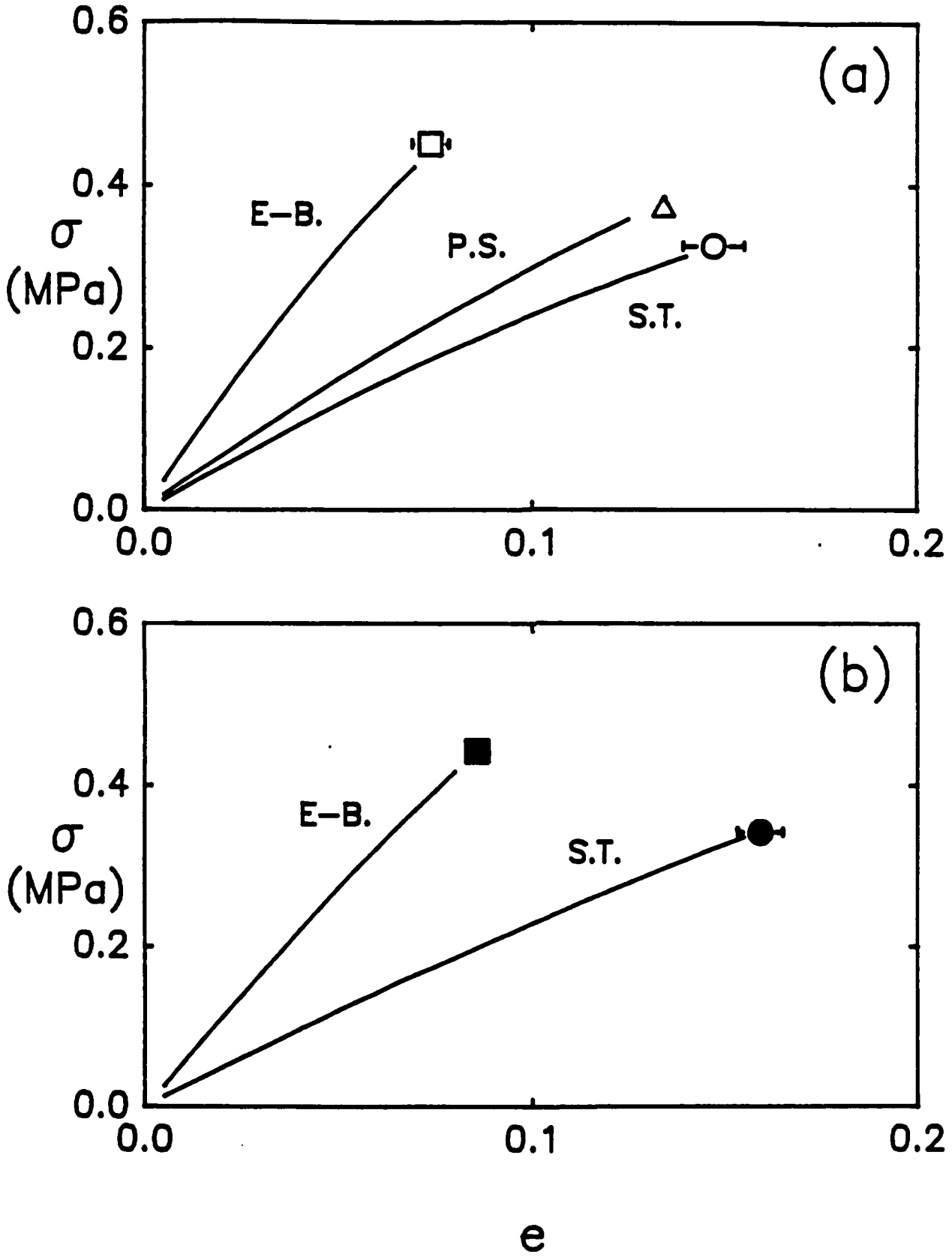

FIGURE 7

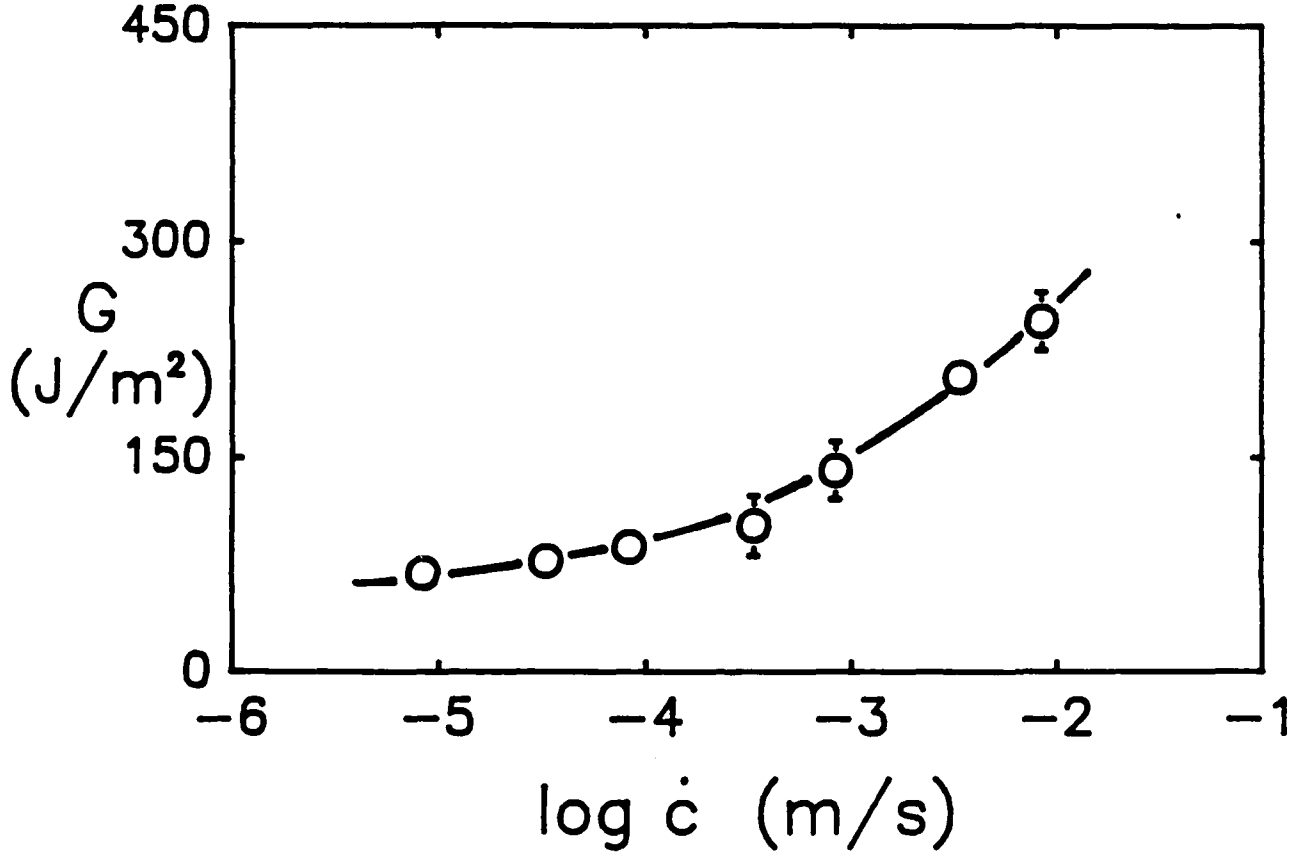

FIGURE 8

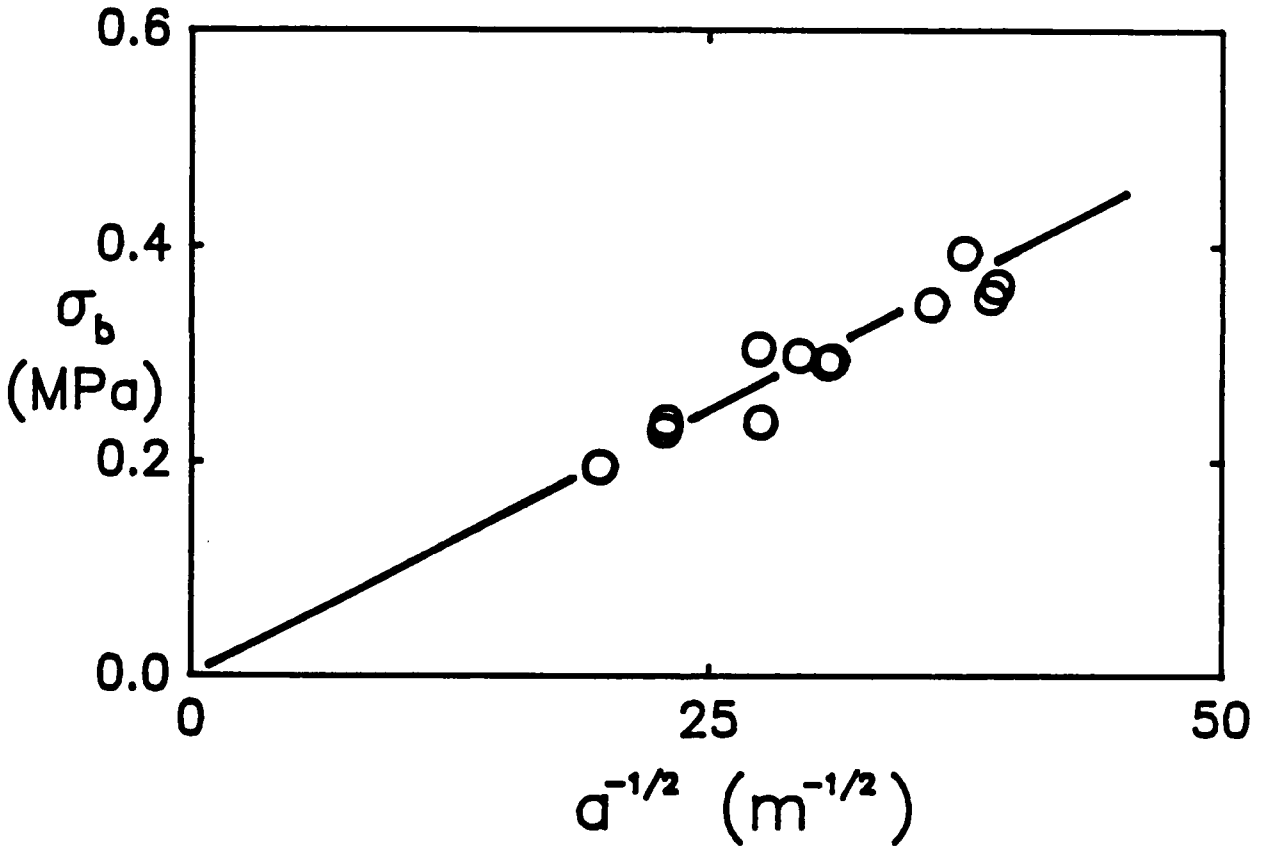

FIGURE 9

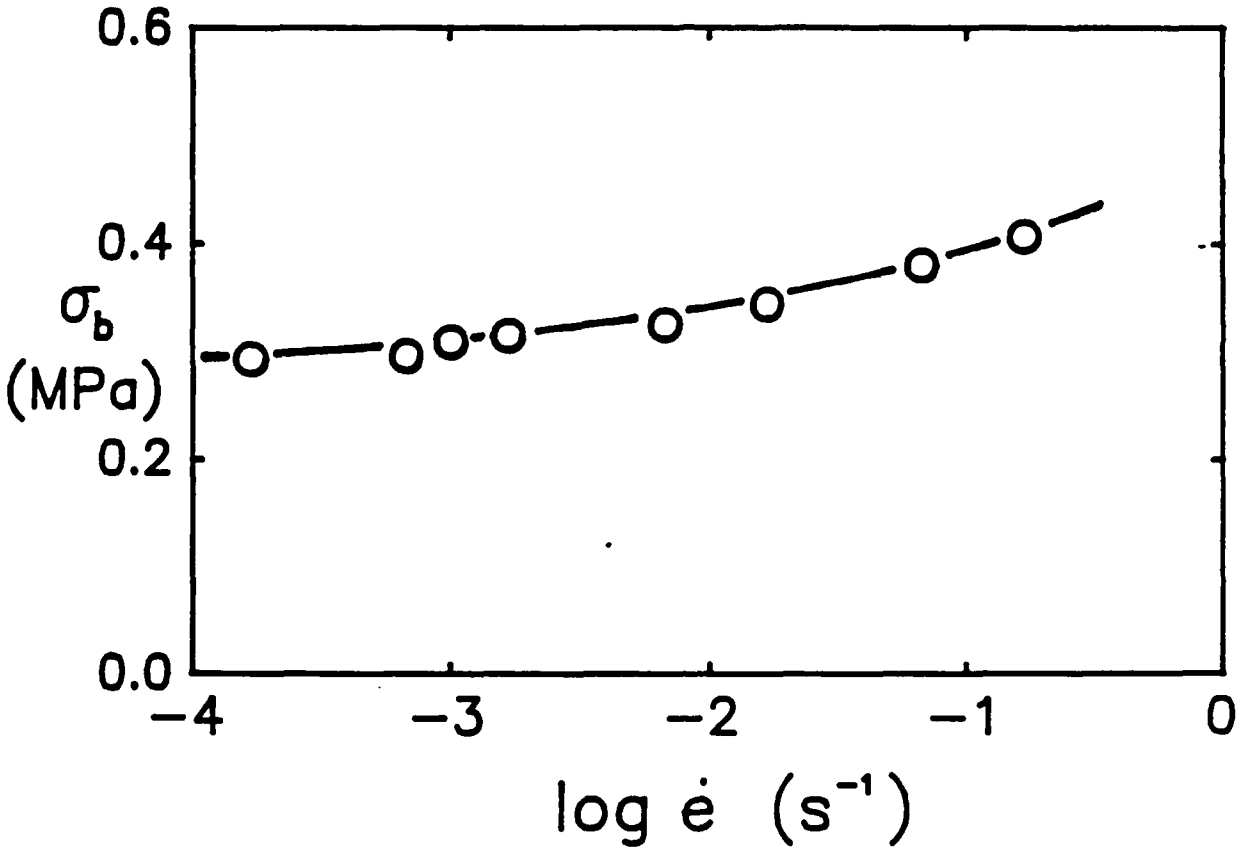

FIGURE 10

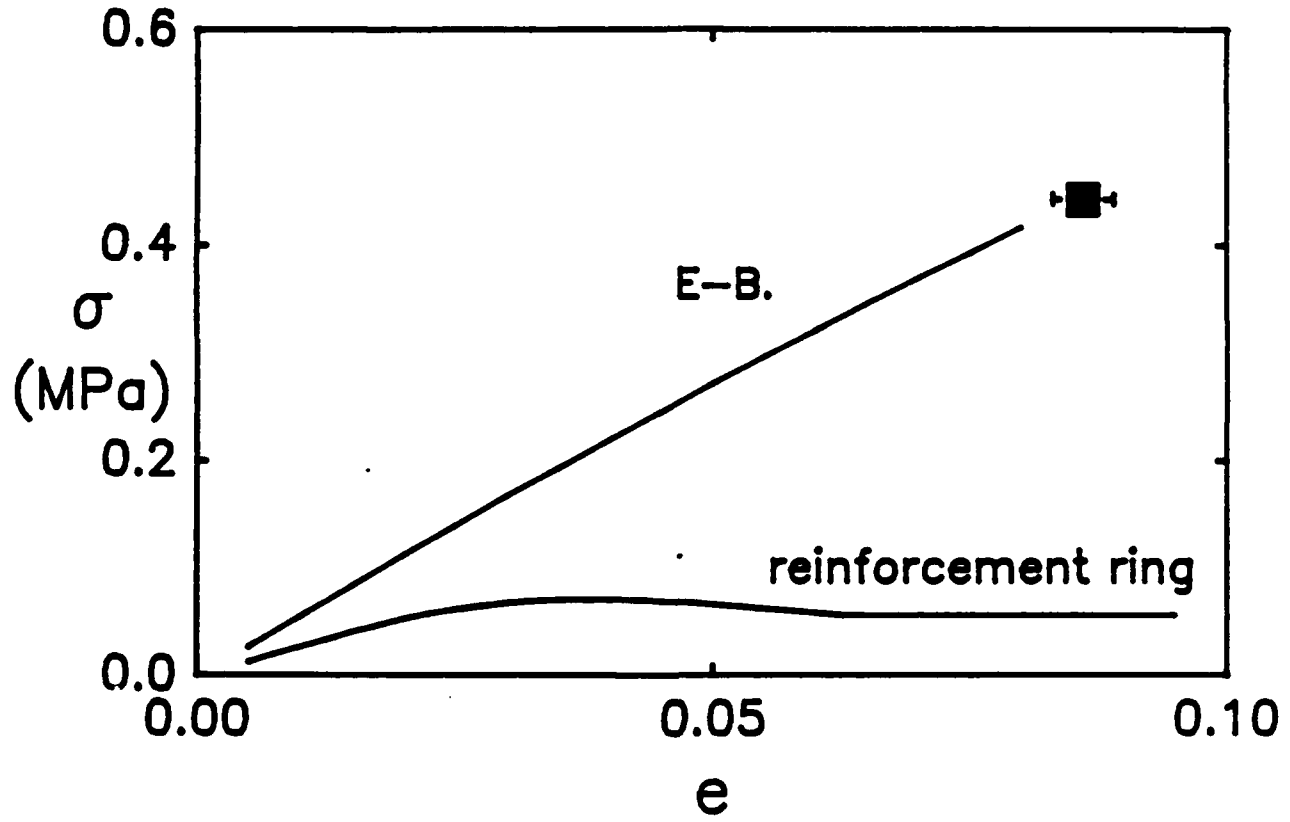

FIGURE 11

(DYN)

DISTRIBUTION LIST

Dr. R.S. Miller
Office of Naval Research
Code 432P
Arlington, VA 22217
(10 copies)

Dr. J. Pastine
Naval Sea Systems Command
Code 06R
Washington, DC 20362

Dr. Kenneth D. Hartman
Hercules Aerospace Division
Hercules Incorporated
Alleghany Ballistic Lab
P.O. Box 210
Cumberland, MD 21502

Mr. Otto K. Heiney
AFATL-DLJC
Elgin AFB, FL 32542

Dr. Merrill K. King
Atlantic Research Corp.
5390 Cherokee Avenue
Alexandria, VA 22312

Dr. R.L. Lou
Aerojet Strategic Propulsion Co.
Bldg. 05025 - Dept 5400 - MS 167
P.O. Box 15699C
Sacramenta, CA 95813

Dr. R. Olsen
Aerojet Strategic Propulsion Co.
Bldg. 05025 - Dept 5400 - MS 167
P.O. Box 15699C
Sacramento, CA 95813

Dr. Randy Peters
Aerojet Strategic Propulsion Co.
Bldg. 05025 - Dept 5400 - MS 167
P.O. Box 15699C
Sacramento, CA 95813

Dr. D. Mann
U.S. Army Research Office
Engineering Division
Box 12211
Research Triangle Park, NC 27709-2211

Dr. L.V. Schmidt
Office of Naval Technology
Code 07CT
Arlington, VA 22217

JHU Applied Physics Laboratory
ATTN: CPIA (Mr. T.W. Christian)
Johns Hopkins Rd.
Laurel, MD 20707

Dr. R. McGuire
Lawrence Livermore Laboratory
University of California
Code L-324
Livermore, CA 94550

P.A. Miller
736 Leavenworth Street, #6
San Francisco, CA 94109

Dr. W. Moniz
Naval Research Lab.
Code 6120
Washington, DC 20375

Dr. K.F. Mueller
Naval Surface Weapons Center
Code R11
White Oak
Silver Spring, MD 20910

Prof. M. Nicol
Dept. of Chemistry & Biochemistry
University of California
Los Angeles, CA 90024

Mr. L. Roslund
Naval Surface Weapons Center
Code R10C
White Oak, Silver Spring, MD 20910

Dr. David C. Sayles
Ballistic Missile Defense
Advanced Technology Center
P.O. Box 1500
Huntsville, AL 35807

(DYN)

DISTRIBUTION LIST

Mr. R. Geisler
ATTN: DY/MS-24
AFRPL
Edwards AFB, CA 93523

Naval Air Systems Command
ATTN: Mr. Bertram P. Sobers
NAVAIR-320G
Jefferson Plaza 1, RM 472
Washington, DC 20361

R.B. Steele
Aerojet Strategic Propulsion Co.
P.O. Box 15699C
Sacramento, CA 95813

Mr. M. Stosz
Naval Surface Weapons Center
Code R10B
White Oak
Silver Spring, MD 20910

Mr. S.F. Palopali
Thiokol Corporation
Elkton Division
P.O. Box 241
Elkton, MD 21921

Dr. Grant Thompson
Morton Thiokol, Inc.
Wasatch Division
MS 240 P.O. Box 524
Brigham City, UT 84302

Dr. R.S. Valentini
United Technologies Chemical Systems
P.O. Box 50015
San Jose, CA 95150-0015

Dr. R.F. Walker
Chief, Energetic Materials Division
DRSMC-LCE (D), B-3022
USA ARDC
Dover, NJ 07801

~~Dr. Janet Weil~~
~~Code 012~~
~~Director, Research Administration~~
~~Naval Postgraduate School~~
~~Monterey, CA 93943~~

Director
US Army Ballistic Research Lab.
ATTN: DRXBR-IBD
Aberdeen Proving Ground, MD 21005

Commander
US Army Missile Command
ATTN: DRSMI-RKL
Walter W. Wharton
Redstone Arsenal, AL 35898

Dr. Ingo W. May
Army Ballistic Research Lab.
ARRADCOM
Code DRXBR - IBD
Aberdeen Proving Ground, MD 21005

Dr. E. Zimet
Office of Naval Technology
Code 071
Arlington, VA 22217

Dr. Ronald L. Derr
Naval Weapons Center
Code 389
China Lake, CA 93555

~~T. Boggs~~
~~Naval Weapons Center~~
~~Code 389~~
~~China Lake, CA 93555~~

Lee C. Estabrook, P.E.
Morton Thiokol, Inc.
P.O. Box 30058
Shreveport, Louisiana 71130

Dr. J.R. West
Morton Thiokol, Inc.
P.O. Box 30058
Shreveport, Louisiana 71130

Dr. D.D. Dillehay
Morton Thiokol, Inc.
Longhorn Division
Marshall, TX 75670

G.T. Bowman
Atlantic Research Corp.
7511 Wellington Road
Gainesville, VA 22065

(DYN)

DISTRIBUTION LIST

R.E. Shenton
Atlantic Research Corp.
7511 Wellington Road
Gainesville, VA 22065

Brian Wheatley
Atlantic Research Corp.
7511 Wellington Road
Gainesville, VA 22065

Mike Barnes
Atlantic Research Corp.
7511 Wellington Road
Gainesville, VA 22065

Mr. G. Edwards
Naval Sea Systems Command
Code 62R32
Washington, DC 20362

Dr. Lionel Dickinson
Naval Explosive Ordinance
Disposal Tech. Center
Code D
Indian Head, MD 20340

C. Dickinson
Naval Surface Weapons Center
White Oak, Code R-13
Silver Spring, MD 20910

Prof. J.T. Dickinson
Washington State University
Dept. of Physics 4
Pullman, WA 99164-2814

Prof. John Deutch
MIT
Department of Chemistry
Cambridge, MA 02139

M.M. Miles
Dept. of Physics
Washington State University
Pullman, WA 99164-2814

~~Dr. E.H. deButts~~
~~Hercules Aerospace Co.~~
~~P.O. Box 27408~~
~~Salt Lake City, UT 84127~~

Dr. T.F. Davidson
Vice President, Technical
Morton Thiokol, Inc.
Aerospace Group
3340 Airport Rd.
Ogden, UT 84405

David A. Flanigan
Director, Advanced Technology
Morton Thiokol, Inc.
Aerospace Group
2475 Washington Blvd.
Ogden, UT 84401

Mr. J. Consaga
Naval Surface Weapons Center
Code R-16
Indian Head, MD 20640

Dr. L.H. Caveny
Air Force Office of Scientific
Research
Directorate of Aerospace Sciences
Bolling Air Force Base
Washington, DC 20332

Naval Sea Systems Command
ATTN: Mr. Charles M. Christensen
NAVSEA-62R2
Crystal Plaza, Bldg. 6, Rm 806
Washington, DC 20362

~~W.G. Roger~~
~~Code 5253~~
~~Naval Ordance Station~~
~~Indian Head, MD 20640~~

Mr. R. Beauregard
Naval Sea Systems Command
SEA 64E
Washington, DC 20362

Dr. Donald L. Ball
Air Force Office of Scientific
Research
Directorate of Chemical &
Atmospheric Sciences
Bolling Air Force Base
Washington, DC 20332

(DYN)

DISTRIBUTION LIST

Dr. Anthony J. Matuszko
Air Force Office of Scientific Research
Directorate of Chemical & Atmospheric Sciences
Bolling Air Force Base
Washington, DC 20332

Dr. H.G. Adolph
Naval Surface Weapons Center
Code R11
White Oak
Silver Spring, MD 20910

Dr. Michael Chaykovsky
Naval Surface Weapons Center
Code R11
White Oak
Silver Spring, MD 20910

U.S. Army Research Office
Chemical & Biological Sciences Division
P.O. Box 12211
Research Triangle Park, NC 27709

J.J. Rocchio
USA Ballistic Research Lab.
Aberdeen Proving Ground, MD 21005-5066

Dr. John S. Wilkes, Jr.
FJSRL/NC
USAF Academy, CO 80840

Dr. H. Rosenwasser
AIR-320R
Naval Air Systems Command
Washington, DC 20361

B. Swanson
INC-4 MS C-346
Los Alamos National Laboratory
Los Alamos, New Mexico 87545

Dr. Joyce J. Kaufman
The Johns Hopkins University
Department of Chemistry
Baltimore, MD 21218

Dr. James T. Bryant
Naval Weapons Center
Code 3205B
China Lake, CA 93555

Dr. A. Nielsen
Naval Weapons Center
Code 385
China Lake, CA 93555

Dr. L. Rothstein
Assistant Director
Naval Explosives Dev. Engineering Dept.
Naval Weapons Station
Yorktown, VA 23691

Dr. M.J. Kamlet
Naval Surface Weapons Center
Code R11
White Oak, Silver Spring, MD 20910

Dr. Henry Webster, III
Manager, Chemical Sciences Branch
ATTN: Code 5063
Crane, IN 47522

Dr. A.L. Slafkosky
Scientific Advisor
Commandant of the Marine Corps
Code RD-1
Washington, DC 20380

(DYN)

DISTRIBUTION LIST

K.D. Pae
High Pressure Materials Research Lab.
Rutgers University
P.O. Box 909
Piscataway, NJ 08854

Dr. John K. Dienes
T-3, B216
Los Alamos National Lab.
P.O. Box 1663
Los Alamos, NM 87544

A.N. Gent
Institute Polymer Science
University of Akron
Akron, OH 44325

Dr. D.A. Shockey
SRI International
333 Ravenswood Ave.
Menlo Park, CA 94025

Dr. R.B. Kruse
Morton Thiokol, Inc.
Huntsville Division
Huntsville, AL 35807-7501

G. Butcher
Hercules, Inc.
P.O. Box 98
Magna, UT 84044

W. Waesche
Atlantic Research Corp.
7511 Wellington Road
Gainesville, VA 22065

Dr. R. Bernecker
Naval Surface Weapons Center
Code R13
White Oak
Silver Spring, MD 20910

Prof. Edward Price
Georgia Institute of Tech.
School of Aerospace Engineering
Atlanta, GA 30332

J.A. Birkett
Naval Ordnance Station
Code 5253K
Indian Head, MD 20640

Prof. R.W. Armstrong
University of Maryland
Dept. of Mechanical Engineering
College Park, MD 20742

Herb Richter
Code 385
Naval Weapons Center
China Lake, CA 93555

J.T. Rosenberg
SRI International
333 Ravenswood Ave.
Menlo Park, CA 94025

G.A. Zimmerman
Aeroject Tactical Systems
P.O. Box 13400
Sacramento, CA 95813

Prof. Kenneth Kuo
Pennsylvania State University
Dept. of Mechanical Engineering
University Park, PA 16802

T.L. Boggs
Naval Weapons Center
Code 3891
China Lake, CA 93555

Ser 432/84/340
Revised January 1985

(DYN)

DISTRIBUTION LIST

Dr. C.S. Coffey
Naval Surface Weapons Center
Code R13
White Oak
Silver Spring, MD 20910

D. Curran
SRI International
333 Ravenswood Avenue
Menlo Park, CA 94025

E.L. Throckmorton
Code SP-2731
Strategic Systems Program Office
Crystal Mall #3, RM 1048
Washington, DC 23076

R.G. Rosemeier
Brimrose Corporation
7720 Belair Road
Baltimore, MD 20742

C. Gotzmer
Naval Surface Weapons Center
Code R-11
White Oak
Silver Spring, MD 20910

G.A. Lo
3251 Hanover Street
B204 Lockheed Palo Alto Research Lab
Palto Alto, CA 94304

R.A. Schapery
Civil Engineering Department
Texas A&M University
College Station, TX 77843

Dr. Y. Gupta
Washington State University
Department of Physics
Pullman, WA 99163

J.M. Culver
Strategic Systems Projects Office
SSPO/SP-2731
Crystal Mall #3, RM 1048
Washington, DC 20376

Prof. G.D. Duvall
Washington State University
Department of Physics
Pullman, WA 99163

Dr. E. Martin
Naval Weapons Center
Code 3858
China Lake, CA 93555

Dr. M. Farber
135 W. Maple Avenue
Monnovia, CA 91016

W.L. Elban
Naval Surface Weapons Center
White Oak, Bldg. 343
Silver Spring, MD 20910

Defense Technical Information Center
Bldg. 5, Cameron Station
Alexandria, VA 22314
(12 copies)

Dr. Robert Polvani
National Bureau of Standards
Metallurgy Division
Washington, D.C. 20234

Director
Naval Research Laboratory
Attn: Code 2627
Washington, DC 20375
(6 copies)

Administrative Contracting
Officer (see contract for
address)
(1 copy)